ARTICLE IN PRESS

Available online at www.sciencedirect.com

SciVerse ScienceDirect

Proceedings of the Combustion Institute xxx (2012) xxx–xxx

Proceedings of the Combustion Institute

www.elsevier.com/locate/proci

An experimental and kinetic modeling investigation on a rich premixed *n*-propylbenzene flame at low pressure

Zhandong Wang [a,b], Yuyang Li [a,b], Feng Zhang [b], Lidong Zhang [b], Wenhao Yuan [b], Yizun Wang [a], Fei Qi [a,b,*]

[a] *State Key Laboratory of Fire Science, University of Science and Technology of China, Hefei, Anhui 230026, PR China*
[b] *National Synchrotron Radiation Laboratory, University of Science and Technology of China, Hefei, Anhui 230029, PR China*

Abstract

A rich premixed flame of *n*-propylbenzene ($\phi = 1.79$) was investigated at low pressure. Synchrotron vacuum ultraviolet photoionization mass spectrometry was used to detect flame species including a lot of radicals, isomers and polycyclic aromatic hydrocarbons (PAHs) and measure their mole fraction profiles. A preliminary kinetic model of *n*-propylbenzene combustion was developed from recently reported toluene and ethylbenzene models [Y.Y. Li et al., *Proc. Combust. Inst.* 33 (2011) 593–600, 617–624] and validated by the experimental results. Rate constants of the important pathways of *n*-propylbenzene consumption, i.e. the H-abstraction reactions by H atom and the benzylic C–C bond dissociation, were calculated theoretically and included in this model. Based on the rate of production analysis and experimental observations, styrene, benzyl and benzene are confirmed as significant intermediates in the *n*-propylbenzene flame. For the formation pathways of PAHs, *n*-propylbenzene flame has a fuel specific pathway to form indene compared to smaller alkylbenzene, which increases the concentrations of indene and indenyl radical. It is concluded that high concentrations of important PAH precursors such as benzyl and indenyl radicals result in the enhanced PAHs formation in this flame compared with smaller alkylbenzenes.

Keywords: *n*-Propylbenzene; Rich premixed flame; Synchrotron VUV photoionization mass spectrometry; Kinetic modeling; PAH formation

1. Introduction

Aromatic hydrocarbons, which largely exist in practical fuels (e.g. 25% by volume in gasoline, 33% in diesel and 16% in jet fuels [1]), have received great attention due to their significant roles in soot production by enhancing the soot precursors such as polycyclic aromatic hydrocarbons (PAHs) [2]. Thus, understanding the combustion properties of this kind of fuel is crucial for the development of clean and efficient engines.

Compared with the most studied aromatic hydrocarbons such as benzene and toluene, *n*-propylbenzene (*n*PB) has longer alkyl chain and higher energy density, and therefore usually serves as a representative aromatic component in jet and diesel surrogate fuels [3,4]. Previous experimental work on *n*PB includes the measurements of global combustion properties such as the ignition delay time [5–7], the laminar flame speed and extinction

* Corresponding author at: National Synchrotron Radiation Laboratory, University of Science and Technology of China, Hefei, Anhui 230029, PR China. Fax: +86 551 5141078.
E-mail address: fqi@ustc.edu.cn (F. Qi).

1540-7489/$ - see front matter © 2012 The Combustion Institute. Published by Elsevier Inc. All rights reserved.
http://dx.doi.org/10.1016/j.proci.2012.05.006

strain rates [8,9] and sooting tendency [10]. Besides, Litzinger et al. [11] studied the oxidation of *n*PB in a plug flow reactor at 1 atm and around 1060 K. They measured mole fractions of the oxidation products and proposed three major reaction routes. Dagaut et al. [12] measured the concentration profiles of 23 species during the oxidation of *n*PB in a jet stirred reactor (JSR) at 1 atm over 900–1250 K. More recently, high temperature oxidation of *n*PB was investigated at high pressure by Gudiyella and Brezinsky [13] in shock tube. However, there are few reports on *n*PB flames containing comprehensive information such as detailed concentration profiles of combustion species, especially intermediate radicals, so that accurate validation of the available kinetic models [6–9,12,13] is limited.

In this work, a rich premixed flame of *n*PB with an equivalence ratio of 1.79 was investigated using synchrotron vacuum ultraviolet photoionization mass spectrometry (SVUV-PIMS). Flame species including radicals, isomers, and PAHs were identified and their mole fractions were evaluated. A preliminary kinetic model of *n*PB combustion was developed from our recently reported toluene and ethylbenzene models [14,15] and validated against the experimental results. The mechanism of fuel consumption and PAHs formation at rich condition was explored based on the experimental and modeling results.

2. Experimental method

The experimental work was performed at National Synchrotron Radiation Laboratory, Hefei, China. The instrument has been described in detail elsewhere [16–18]. The rich *n*PB/Ar/O_2 flame at 30 Torr (equal to 40 mbar) was stabilized on a McKenna burner with a diameter of 6.0 cm. The flow rates of Ar and O_2 were 1.523 and 1.326 standard liter per minute (SLM), respectively. The flow rate of liquid *n*PB was 1.234 ml/min (equal to 0.198 SLM in the gas phase). Therefore the equivalence ratio was calculated to be 1.79. The inlet mass flow rate and cold-flow (300 K) velocity were 3.343×10^{-3} g s^{-1} cm^{-2} and 50 cm s^{-1}, respectively.

Intermediates identification and mole fraction evaluation were based on previously reported methods [17,19]. The photoionization cross sections (PICSs) of most species were taken from literatures and are available in our online database [20]. For species with unknown values, their PICSs were estimated from molecules with similar structures. The uncertainties of measured mole fractions are about ±10% for major species, ±25% for intermediates with known PICSs, and a factor of 2 for those with estimated PICSs. It should be noted that the uncertainties close to the burner surface for some species are much larger due to the perturbation of the sampling nozzle. The flame temperature profile was measured by a 0.1-mm-diameter Pt-6%Rh/Pt-30%Rh thermocouple coated with Y_2O_3–BeO anti-catalytic ceramic [21,22], and was calibrated for radiative heat loss [23] and cooling effects of sampling nozzle [24]. The uncertainty of the maximum flame temperature was estimated to be ±100 K.

3. Kinetic modeling

The preliminary kinetic model for *n*PB combustion is constructed based on our previous developed aromatic model which has been validated against the pyrolysis of toluene [25], premixed flames of toluene [14] and ethylbenzene [15], and the details about the base model is discussed in the Supplemental data. The development of the sub-mechanism of *n*PB will be described below. Figure 1 shows the structures, names and nomenclatures of some important

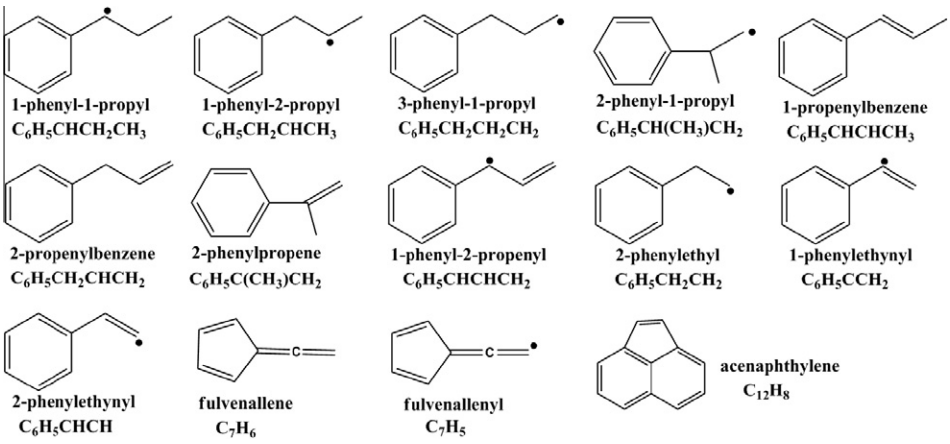

Fig. 1. Structures, names and nomenclatures of some mentioned species in this work.

Please cite this article in press as: Z. Wang et al., *Proc. Combust. Inst.* (2012), http://dx.doi.org/10.1016/j.proci.2012.05.006

Table 1
Rate constants of some selected reactions in sub-mechanism of *n*PB combustion. $k = AT^n \exp(-E/RT)$. The units are in cm^3, mol, s, cal.

No.	Reactions	A	n	E	Refs
1	$C_6H_5C_3H_7 + H = C_6H_5CHCH_2CH_3 + H_2$	5.75×10^7	1.85	5599	a
2	$C_6H_5C_3H_7 + H = C_6H_5CH_2CHCH_3 + H_2$	7.97×10^7	1.86	6819	a
3	$C_6H_5C_3H_7 + H = C_6H_5CH_2CH_2CH_2 + H_2$	6.31×10^6	2.23	8641	a
4	$C_6H_5C_3H_7 + OH = C_6H_5CHCH_2CH_3 + H_2O$	3.00×10^6	2.00	−1520	b
5	$C_6H_5C_3H_7 + OH = C_6H_5CH_2CHCH_3 + H_2O$	2.60×10^6	2.00	−770	b
6	$C_6H_5C_3H_7 + OH = C_6H_5CH_2CH_2CH_2 + H_2O$	2.67×10^6	2.00	450	b
7	$C_6H_5C_3H_7 + H = C_6H_6 + nC_3H_7$	5.78×10^{13}	0.00	8087	c
8	$C_6H_5C_3H_7 = C_6H_5CH_2 + C_2H_5$	6.11×10^{96}	−23.78	118,160	a
9	$C_6H_5C_3H_7 = C_6H_5CH_2CH_2 + CH_3$	6.11×10^{96}	−23.78	130,160	est
10	$C_6H_5 + nC_3H_7 (+M) = C_6H_5C_3H_7 (+M)$	2.33×10^{14}	−0.28	−191	d
	Low pressure limit	6.73×10^{83}	−19.22	14,980	
	Troe parameters: 0.5918 320.14 1858.2 5395.0				
11	$C_6H_5CHCH_2CH_3 = C_6H_5C_2H_3 + CH_3$	1.30×10^{13}	0.00	35,900	b
12	$C_6H_5CHCH_2CH_3 = C_6H_5CHCHCH_3 + H$	3.00×10^{13}	0.00	50,500	b
13	$C_6H_5CH_2CHCH_3 = C_6H_5CHCH_2CH_3$	2.00×10^{-15}	6.56	13,502	a
14	$C_6H_5CH_2CHCH_3 = C_6H_5CHCHCH_3 + H$	1.50×10^{-17}	7.10	13,119	a
15	$C_6H_5CH_2CHCH_3 = C_6H_5CH_2CHCH_2 + H$	2.10×10^{-17}	7.40	13,140	a
16	$C_6H_5CH_2CHCH_3 = C_6H_5 + C_3H_6$	5.00×10^{-21}	8.22	15,514	a
17	$C_6H_5CH_2CHCH_3 = C_6H_5CH(CH_3)CH_2$	5.56×10^6	0.68	7780	a
18	$C_6H_5CH_2CH_2CH_2 = C_6H_5CH_2 + C_2H_4$	2.00×10^{13}	0.00	28,700	b
19	$C_6H_5CH_2CH_2CH_2 = C_6H_5CH_2CHCH_2 + H$	3.00×10^{13}	0.00	38,000	b
20	$C_6H_5CH(CH_3)CH_2 = C_6H_5C_2H_3 + CH_3$	2.00×10^{13}	0.00	31,000	b
21	$C_6H_5CH(CH_3)CH_2 = C_6H_5 + C_3H_6$	2.00×10^{13}	0.00	38,500	b
22	$C_6H_5CH(CH_3)CH_2 = C_6H_5C(CH_3)CH_2 + H$	1.60×10^{13}	0.00	34,300	b
23	$C_6H_5CHCHCH_2 + H (+M) = C_6H_5CHCHCH_3 (+M)$	2.00×10^{14}	0.00	0	e
	Low pressure limit	1.33×10^{60}	−12.00	5968	
	Troe parameter: 0.020 1096.6 1096.6 6859.5				
24	$C_6H_5CHCHCH_2 + H = C_6H_5CH_2CHCH_2$	1.00×10^{14}	0.00	0	b
25	$C_9H_8 + H = C_6H_5CHCHCH_2$	1.00×10^{13}	0.00	0	est

[a] Calculated in this work.
[b] Ref. to [42].
[c] Ref. to $C_6H_5C_2H_5 + H = C_6H_6 + C_2H_5$.
[d] Ref. to $C_6H_5 + CH_3 (+M) = C_6H_5CH_3 (+M)$.
[e] Ref. to $aC_3H_5 + H (+M) = C_3H_6 (+M)$.

species. Initial reactions of *n*PB dominantly occur at the side chain since the bond dissociation energies (BDEs) of C–C and C–H bonds are lower than those on the benzene ring. Table 1 lists some important reactions of the sub-mechanism of *n*PB combustion and their rate constants with Arrhenius parameters. Similar to the mechanism proposed by Dagaut et al. [12], three kinds of reactions are considered as *n*PB consumption pathways in this model.

(1) H-abstracted by H, O atom and OH radical etc. to produce three C_9H_{11} radicals including 1-phenyl-1-propyl, 1-phenyl-2-propyl and 3-phenyl-1-propyl radicals. Further decomposition reactions of these C_9H_{11} radicals are also listed in Table 1.
(2) Displacement of the *n*-propyl group by H to form benzene.
(3) Dissociation of C–C bond on the side chain to form phenyl + *n*-propyl, benzyl + ethyl and 2-phenylethyl + methyl, and H elimination from the side chain to produce 1-phenyl-1-propyl, 1-phenyl-2-propyl and 3-phenyl-1-propyl radicals.

The rate constants of *n*PB reactions were usually referred to analogue reactions of toluene and propane, etc [12,13]. In this work, the rate constants of H attack on the side chain (R1–R3 listed in Table 1) and benzylic C–C bond scission (R8) of *n*PB were calculated. The H attack reactions were investigated by the composite CBS-QB3 method [26,27]. The barrierless C–C bond dissociation of *n*PB was stepwisely (with a 0.2 Å stepsize) optimized along the C–C bond length at B3LYP/6-311g(2d,d,p). Then the potential curve was scaled by the CBS-QB3 dissociation energy. Besides, both decomposition and isomerization channels of 1-phenyl-2-propyl radical (R13–R17) were also calculated at the CBS-QB3 level. All *ab initio* calculations were performed with the Gaussian 09 program package [28]. The calculated energy profiles of H-abstraction and

unimolecular decomposition of *n*PB are shown in Figs. S1 and S2 in the Supplemental data. Based on the computed reaction pathways, the rate constants were calculated by the RRKM/Master Equation method for unimolecular reactions and variational transition state theory for H attack reactions with the ChemRate program [29]. The barrierless C–C dissociation was treated variationally [30]. Low frequency vibrational modes were replaced by hindered rotors with symmetric hindrance potential functions. The Lennard-Jones parameters were estimated by the empirical rules [31], i.e. $\sigma = 6.66$ Å for *n*PB and 6.61 Å for the 1-phenyl-2-propyl radical, $\varepsilon = 522$ K for both. Argon was chosen as the bath gas ($\sigma = 3.47$, $\varepsilon = 114$ K). These calculated rate constants are included in the kinetic model. The kinetic modeling was performed by using the PREMIX Code of the Chemkin-PRO software [32].

4. Results and discussion

4.1. n-Propylbenzene consumption

Fig. 2 presents the measured and simulated mole fraction profiles of major species along with the temperature profile of the investigated flame. It is observed that *n*PB is almost consumed at 5.5 mm while oxygen runs out at ~11 mm. Residual oxygen is consumed by the combustion intermediates after the complete consumption of the fuel. The mole fraction of Ar decreases from the burner surface due to the mole expansion effect, then becomes almost constant after the reaction zone. Because of the rich flame condition, the concentrations of incomplete oxidation products such as CO and H_2 are very high at the postflame zone.

Dozens of combustion intermediates including a lot of radicals, isomers and PAHs were detected in this work as listed in Table S1 in the Supplemental data, which are similar to the intermediates in our recently reported rich ethylbenzene flame ($\phi = 1.79$) [15,33]. The measured and predicted mole fraction profiles of some important intermediates involved in the consumption of *n*PB are displayed in Fig. 3. The mole fraction uncertainties are ±25% for ethylbenzene ($C_6H_5C_2H_5$), styrene ($C_6H_5C_2H_3$), phenylacetylene ($C_6H_5C_2H$), toluene ($C_6H_5CH_3$), benzene (C_6H_6), 1,3-butadiyne, ethylene and acetylene, and a factor of 2 for phenol (C_6H_5OH), benzyl radical ($C_6H_5CH_2$), fulvenallene (C_7H_6), fulvenallenyl radical (C_7H_5), 1,3-cyclopentadiene (C_5H_6), cyclopentadienyl radical (C_5H_5), propargyl radical (C_3H_3) and ethyl radical (C_2H_5). Based on the rate of production (ROP) analysis, the reaction network of *n*PB consumption is displayed in Fig. 4. The following discussion will be organized by the three kinds of primary reaction pathways. Further reactions of corresponding primary products will be included in the discussion of each primary pathway.

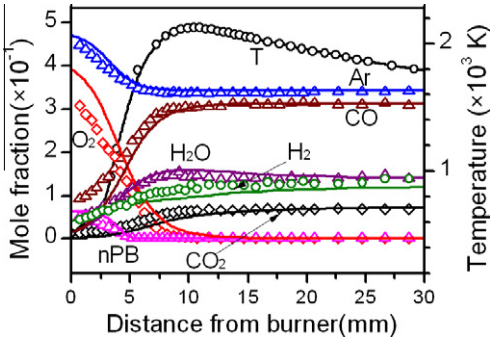

Fig. 2. Measured (open symbols) and predicted (solid lines) mole fraction profiles of the major flame species and the temperature profile.

4.1.1. H-abstraction by radical attack

In this flame, H-abstraction at three sites of the side chain by H atom and OH radical are important consumption channels of *n*PB ($C_6H_5C_3H_7$), producing 1-phenyl-1-propyl ($C_6H_5CHCH_2CH_3$, 19%), 1-phenyl-2-propyl ($C_6H_5CH_2CHCH_3$, 16%) and 3-phenyl-1-propyl ($C_6H_5CH_2CH_2CH_2$, 11%) radicals. These pathways also control the formation of these C_9H_{11} radicals, while the C–H dissociation of the side chain has minor contribution. Due to their thermal instabilities and quenching effects during sampling, these radicals were hardly detected. 1-Phenyl-1-propyl radical mainly dissociates into styrene and CH_3 by β-C–C scission after its formation. Litzinger et al. [11] proposed that 1-phenyl-2-propyl radical could isomerize into 2-phenyl-1-propyl radical ($C_6H_5CH(CH_3)CH_2$) by phenyl shift. Our calculated results confirm this mechanism. As shown in Fig. 5, the phenyl shift reaction has the lowest energy barrier among all the studied reaction pathways of 1-phenyl-2-propyl radical. Then the 2-phenyl-1-propyl radical is further converted to styrene through β-C–C scission. This reaction sequence is included in the present model and shown in the overall form in Fig. 4. Similar to 1-phenyl-1-propyl, the 3-phenyl-1-propyl radical mainly decomposes through β-C–C scission to produce benzyl and ethylene. Besides, the H-elimination of the three C_9H_{11} radicals will produce 1-propenylbenzene and 2-propenylbenzene.

Based on the ROP analysis and the observed extremely high concentration (Fig. 3b), we conclude that styrene is the most important decomposition product from the C_9H_{11} radicals. Styrene is consumed by several pathways, such as H-abstraction by H atom to produce two C_8H_7 radicals, i.e., 1-phenylethynyl ($C_6H_5CCH_2$) and 2-phenylethynyl (C_6H_5CHCH); and reactions

Please cite this article in press as: Z. Wang et al., *Proc. Combust. Inst.* (2012), http://dx.doi.org/10.1016/j.proci.2012.05.006

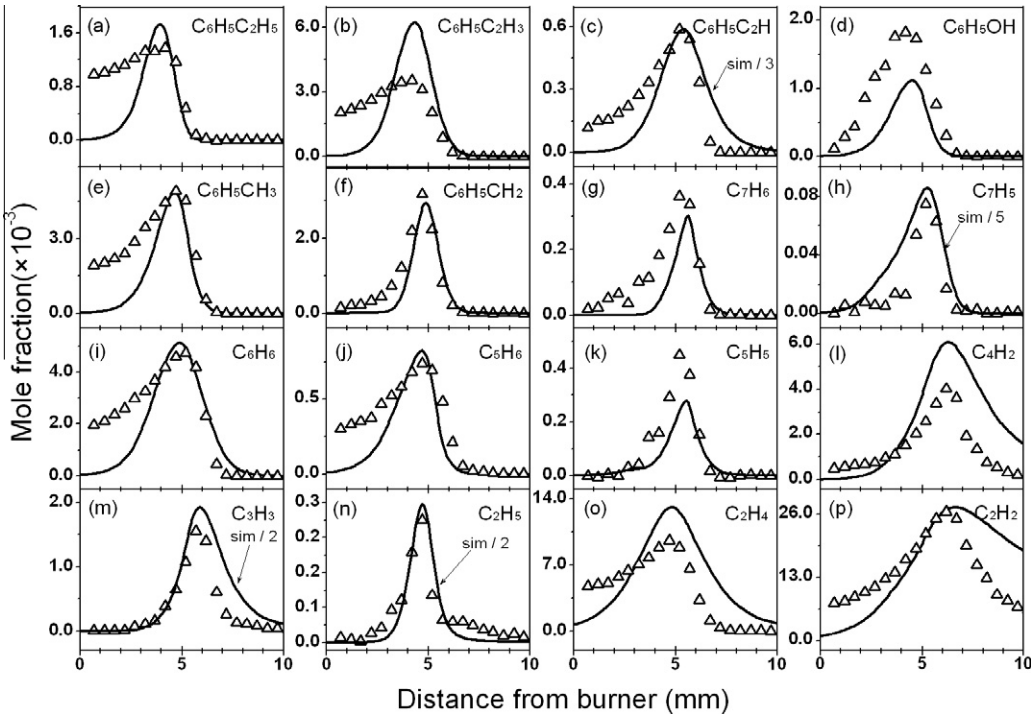

Fig. 3. Measured (open symbols) and predicted (solid lines) mole fraction profiles of some selected C2–C8 intermediates.

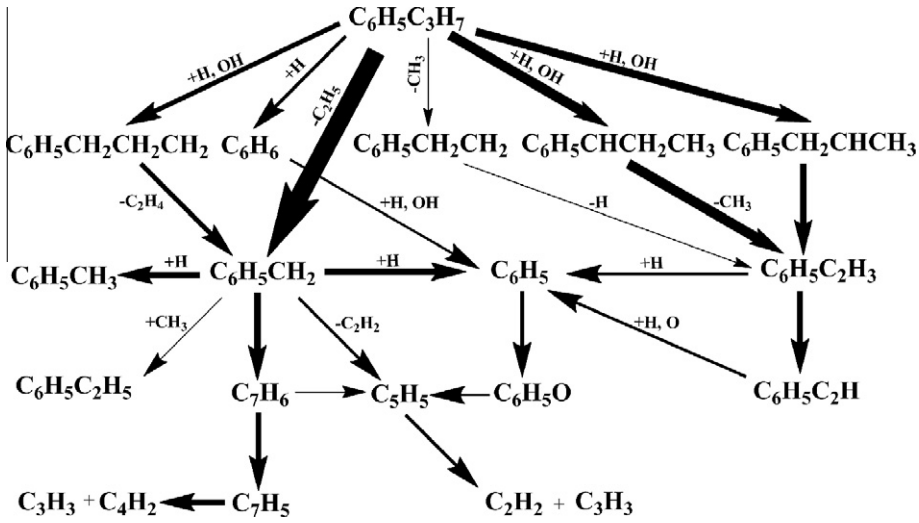

Fig. 4. Reaction network of *n*PB consumption. Thickness of each arrow represents the flux of corresponding reaction(s).

with H atom to form benzene + C_2H_3 and phenyl + C_2H_4. β-C–H scission of C_8H_7 radicals is the main source of phenylacetylene formation. Phenylacetylene is mainly consumed by H and O atoms to produce phenyl radical, as shown in Fig. 4. As can be seen from Fig. 3b and c, this model reproduces the peak positions of styrene and phenylacetylene, but overpredicts the maximum mole fractions (X_{max}).

4.1.2. Displacement of n-propyl group by H atom

The second important consumption pathway discussed in the kinetic modeling section is the displacement of the *n*-propyl group by H atom. In

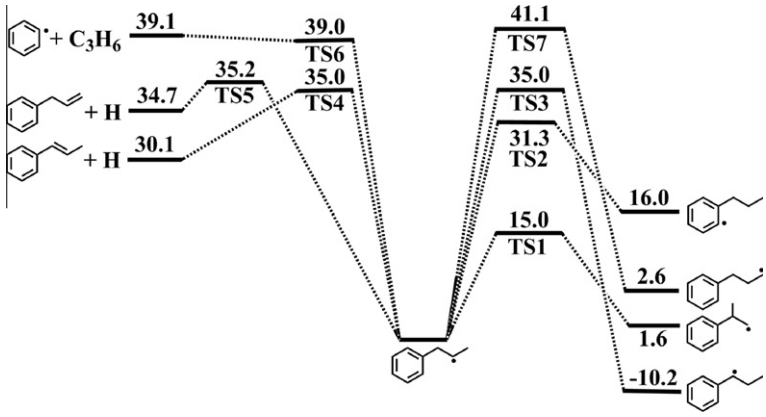

Fig. 5. Isomerization and decomposition pathways of 1-phenyl-2-propyl radical calculated at CBS-QB3 level (unit: kcal/mol).

this flame, this channel only plays a minor role in the *n*PB consumption with a contribution of 7%. However, this reaction is one of the main channels of benzene formation, especially at early stage of the flame, while the H + toluene and H + styrene reactions have comparable contributions to benzene formation over the whole reaction zone.

Benzene is mainly consumed by H-abstraction via H atom and OH radical to produce phenyl radical, as shown in Fig. 4. Phenyl oxidation controls the formation of phenoxyl radical (C_6H_5O), while the phenoxyl radical reacting with H is the dominant channel of phenol formation. The phenol decomposition forms 1,3-cyclopentadiene, which is consumed by radical attack to produce cyclopentadienyl radical. Due to the strong interconversion between phenoxyl and phenol, the reactions of phenoxyl can be tentatively validated by comparing the predicted and measured results of phenol (Fig. 3d) though phenoxyl and phenyl themselves are hardly detected. Unimolecular decomposition of phenoxyl is the most important formation channel for cyclopentadienyl radical which is further decomposed into propargyl radical and acetylene.

4.1.3. Cleavage of the side chain

Besides the above two kinds of reactions, the cleavage of the side chain plays an important role in *n*PB decomposition. In particular, the cleavage of benzylic C–C bond has extraordinarily large contribution compared with other bond scissions, because the BDE of this bond is at least 10 kcal/mol lower than other bonds in *n*PB molecule [34]. It is the most significant decomposition reaction of *n*PB in this flame and has almost equal contribution (44%) with the sum of all H-abstraction reactions (see Fig. 4). This channel produces benzyl and ethyl radicals. As shown in Fig. 3f, the predicted mole fraction profile of benzyl radical is in fairly good agreement with the measured results. The discrepancy between the predicted and measured results of ethyl radical (Fig. 3n) is probably caused by its large experimental uncertainties due to the unreliable PICS. Benzyl radical is primarily produced from the cleavage of benzylic C–C bond (77%), and partly from the β-C–C scission of 3-phenyl-1-propyl (18%). Because of the great carbon flux received, its concentration ($X_{max} = 3.18 \times 10^{-3}$) in this flame is even higher than those in the rich toluene and ethylbenzene flames with similar flame conditions [14,15]. The association reaction between benzyl and H is one of the important consumption pathway of benzyl (22%) and also the dominant channel for toluene formation, leading to a high concentration of toluene ($X_{max} = 4.92 \times 10^{-3}$), as shown in Fig. 3e. Similarly, the reaction of benzyl and CH_3 controls the ethylbenzene formation and consumes about 6% of benzyl. Further reactions of toluene and ethylbenzene consumption have been investigated in our previous studies [14,15] and will not be discussed here. Besides, 25% of benzyl radical is consumed by reacting with H atom to produce phenyl radical and CH_3.

Benzyl can also suffer unimolecular decomposition reactions to produce fulvenallene (C_7H_6) + H and cyclopentadienyl + acetylene. The computational study by da Silva et al. [35] indicated that the former has much higher branching ratio than the latter. In this study, the one producing fulvenallene + H also has higher carbon flux than that producing C_5H_5 and C_2H_2, as shown in Fig. 4. The mole fraction of fulvenallene is displayed in Fig. 3g. Several decomposition channels of fulvenallene and their rate constants have been theoretically studied previously [36–38]. In this work, fulvenallene mainly goes to fulvenallenyl radical (C_7H_5) via H-abstraction and unimolecular decomposition, and also the fulvenallenyl radical

Please cite this article in press as: Z. Wang et al., *Proc. Combust. Inst.* (2012), http://dx.doi.org/10.1016/j.proci.2012.05.006

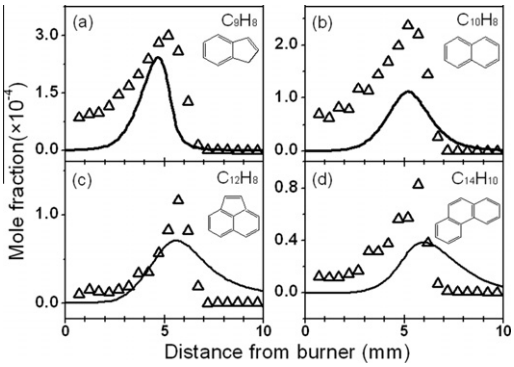

Fig. 6. Measured (open symbols) and predicted (solid lines) mole fraction profiles of (a) indene, (b) naphthalene, (c) acenaphthylene and (d) phenanthrene.

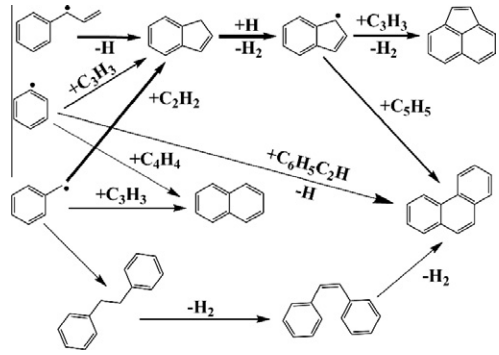

Fig. 7. Reaction network of PAH formation. Thickness of each arrow represents the flux of corresponding reaction(s) and is in a much smaller scale as the arrow thicknesses in Fig. 4.

was detected in this work (Fig. 3h). The dominant consumption route of the fulvenallenyl radical is to form C_4H_2 and C_3H_3.

In a word, the rich *n*PB flame results in high concentrations of styrene, benzyl, and benzene, which are further consumed to smaller species, as shown in Fig. 4. The results of these small intermediates are shown in Fig. 3. Their consumption routes in this flame is quite similar to those in the rich toluene and ethylbenzene flames [14,15] and will not be discussed in detail here.

4.2. PAHs formation

Rich premixed flame is a good system to investigate the mechanism of PAHs formation since small precursors for ring enlargement like acetylene, 1,3-butadiyne, vinylacetylene and the corresponding radicals in HACA mechanism [39], and propargyl and cyclopentadienyl radicals in the resonantly stabilized radical addition mechanism [40,41] have high concentrations (see Fig. 3).

Figure 6 shows the measured and predicted mole fraction profiles of some typical PAHs including indene (C_9H_8), naphthalene ($C_{10}H_8$), acenaphthylene ($C_{12}H_8$) and phenanthrene ($C_{14}H_{10}$). The predictions of these species are reasonably good considering the experimental uncertainties of ±25% for indene and a factor of 2 for the rest PAHs. Figure 7 illustrates the main channels forming these species according to the ROP analysis.

Compared with our recently reported rich toluene and ethylbenzene flames with almost identical flame conditions [14,15], most observed PAHs in this flame have slightly higher concentrations. For example, the X_{max} of indene is around 1.5 times as that in the ethylbenzene flame where its formation is mainly from the HACA channel on benzyl and the propargyl addition to phenyl. Previous study [13] have proposed that a fuel specific pathway for indene formation exists in *n*PB combustion. As shown in Fig. 7, the monocyclic C_9H_9 radical ($C_6H_5CHCHCH_2$) produced from the H-abstraction of 1-propenylbenzene and 2-propenylbenzene can undergo a cyclization reaction forming a bicyclic C_9H_9 radical which produces indene by β-C–H scission. In this flame, this pathway contributes about 35% to indene formation. The consumption of indene mainly produces indenyl radical (C_9H_7) which is involved in the formation of larger PAHs such as acenaphthylene and phenanthrene.

For other three PAHs in Fig. 6, the main formation channels are similar to those in the rich ethylbenzene flame. The propargyl addition to benzyl (73%) and the reaction of vinylacetylene with phenyl (17%) are main sources for naphthalene formation. Acenaphthylene is dominantly formed from the propargyl addition to indenyl. Phenanthrene is mainly formed from the combination of cyclopentadienyl and indenyl radical, the combination of phenyl and phenylacetylene and the two-step dehydrogenation of bibenzyl which is dominantly formed from the self-combination of benzyl.

In a word, the higher concentrations of these PAHs in this flame than in the rich ethylbenzene flame are caused by the enhanced formation of PAH precursors such as benzyl and indenyl. This observation is a possible explanation for the higher sooting tendency of *n*PB than toluene and ethylbenzene, as reported by McEnally and Pfefferle [10].

5. Conclusions and perspectives

A rich premixed *n*PB flame was studied at low pressure by using SVUV-PIMS. The flame species including a lot of radicals, isomers and PAHs were identified and their mole fraction profiles were measured. A preliminary kinetic model was

Please cite this article in press as: Z. Wang et al., *Proc. Combust. Inst.* (2012), http://dx.doi.org/10.1016/j.proci.2012.05.006

developed and validated against the experimental results. The model reproduces the measured mole fraction profiles of most intermediates. The ROP analysis shows that *n*PB is dominantly consumed by H-abstraction on the side chain and cleavage of benzylic C–C bond. Styrene, benzyl, and benzene are important intermediates in the *n*PB flame. Some PAHs have slightly higher concentrations in this flame than in the rich toluene and ethylbenzene flames because of the increased concentrations of PAH precursors such as benzyl and indenyl. More experimental investigations on various conditions such as pyrolysis, lean and stoichiometric flames of *n*PB are desired for the further development and validation of the *n*PB model.

Acknowledgements

This research was supported by National Basic Research Program of China (973 Program) (2012CB719701), Chinese Universities Scientific Fund (WK2310000010), Natural Science Foundation of China (50925623, 51106146), China Postdoctoral Science Foundation (20100480047, 201104326), and Chinese Academy of Sciences. We thank Zhanjun Cheng, Hanfeng Jin for their help in the experiment, and Jianghuai Cai for useful discussion. The numerical calculations have been done on the supercomputing system in the USTC Supercomputing Center.

Appendix A. Supplementary data

Supplementary data associated with this article can be found, in the online version, at http://dx.doi.org/10.1016/j.proci.2012.05.006.

References

[1] Northrop Grumman, Northrop Grumman Petroleum Product Survey Reports, updated annually, available at http://www.pps.ms.northropgrumman.com/.
[2] C.S. McEnally, L.D. Pfefferle, B. Atakan, K. Kohse-Höinghaus, *Prog. Energy Combust. Sci.* 32 (2006) 247–294.
[3] P. Dagaut, M. Cathonnet, *Prog. Energy Combust. Sci.* 32 (2006) 48–92.
[4] W.J. Pitz, C.J. Mueller, *Prog. Energy Combust. Sci.* 37 (2011) 330–350.
[5] A. Roubaud, R. Minetti, L.R. Sochet, *Combust. Flame* 121 (2000) 535–541.
[6] H. Wang, in: 7th US National Technical Meeting of the Combustion Institute, 2011.
[7] D. Darcy, C.J. Tobin, K. Yasunaga, et al., *Combust. Flame* 159 (2012) 2219–2232.
[8] C.S. Ji, E. Dames, H. Wang, F.N. Egolfopoulos, *Combust. Flame* 159 (2012) 1070–1081.
[9] S.H. Won, S. Dooley, F.L. Dryer, Y.G. Ju, *Proc. Combust. Inst.* 33 (2011) 1163–1170.
[10] C.S. McEnally, L.D. Pfefferle, *Combust. Flame* 148 (2007) 210–222.
[11] T.A. Litzinger, K. Brezinsky, I. Glassman, *Combust. Sci. Technol.* 50 (1986) 117–133.
[12] P. Dagaut, A. Ristori, A. El Bakali, M. Cathonnet, *Fuel* 81 (2002) 173–184.
[13] S. Gudiyella, K. Brezinsky, *Combust. Flame* 159 (2012) 940–958.
[14] Y.Y. Li, J.H. Cai, L.D. Zhang, T. Yuan, K.W. Zhang, F. Qi, *Proc. Combust. Inst.* 33 (2011) 593–600.
[15] Y.Y. Li, J.H. Cai, L.D. Zhang, J.Z. Yang, Z.D. Wang, F. Qi, *Proc. Combust. Inst.* 33 (2011) 617–624.
[16] F. Qi, R. Yang, B. Yang, et al., *Rev. Sci. Instrum.* 77 (2006) 084101.
[17] Y.Y. Li, L.D. Zhang, Z.Y. Tian, et al., *Energy Fuels* 23 (2009) 1473–1485.
[18] Y.Y. Li, F. Qi, *Acc. Chem. Res.* 43 (2009) 68–78.
[19] Z.D. Wang, A. Lucassen, L.D. Zhang, J.Z. Yang, K. Kohse-Höinghaus, F. Qi, *Proc. Combust. Inst.* 33 (2011) 415–423.
[20] Photonionization Cross Section Database (Version 1.0), National Synchrotron Radiation Laboratory, Hefei, China, 2011, available at http://flame.nsrl.ustc.edu.cn/en/database.htm.
[21] J.H. Kent, *Combust. Flame* 14 (1970) 279–281.
[22] R.A. Shandross, J.P. Longwell, J.B. Howard, *Combust. Flame* 85 (1991) 282–284.
[23] R.M. Fristrom, *Flame Structure and Processes*, Oxford, New York, 1995, p. 119.
[24] A.T. Hartlieb, B. Atakan, K. Kohse-Höinghaus, *Combust. Flame* 121 (2000) 610–624.
[25] L.D. Zhang, J.H. Cai, T.C. Zhang, F. Qi, *Combust. Flame* 157 (2010) 1686–1697.
[26] J.A. Montgomery, M.J. Frisch, J.W. Ochterski, G.A. Petersson, *J. Chem. Phys.* 112 (2000) 6532–6542.
[27] J.A. Montgomery, M.J. Frisch, J.W. Ochterski, G.A. Petersson, *J. Chem. Phys.* 110 (1999) 2822–2827.
[28] M.J. Frisch et al., Gaussian 09, Revision B.01, Gaussian, Inc., Wallingford CT, 2010.
[29] V. Mokrushin, V. Bedanov, W. Tsang, M. Zachariah, V. Knyazev, ChemRate, Version 1.5.8; National Institute of Standard and Technology: Gaithersburg, MD, 2009.
[30] G. da Silva, J.W. Bozzelli, *J. Phys. Chem. A* 112 (2008) 3566–3575.
[31] R.G. Gilbert, S.C. Smith, *Theory of Unimolecular and Recombination Reactions*, Blackwell, Oxford, UK, 1990.
[32] CHEMKIN-PRO 15092, Reaction Design: San Diego, 2009.
[33] Y.Y. Li, L.D. Zhang, T. Yuan, et al., *Combust. Flame* 157 (2010) 143–154.
[34] Y.-R. Luo, *Comprehensive Handbook of Chemical Bond Energies*, CRC Press, Boca Raton, FL, 2007.
[35] G. da Silva, J.A. Cole, J.W. Bozzelli, *J. Phys. Chem. A* 113 (2009) 6111–6120.
[36] C. Cavallotti, M. Derudi, R. Rota, *Proc. Combust. Inst.* 32 (2009) 115–121.
[37] G. da Silva, J.W. Bozzelli, *J. Phys. Chem. A* 113 (2009) 12045–12048.

[38] D. Polino, C. Cavallotti, *J. Phys. Chem. A* 115 (2011) 10281–10289.
[39] M. Frenklach, H. Wang, *Proc. Combust. Inst.* 23 (1991) 1559–1566.
[40] M.B. Colket, D.J. Seery, *Proc. Combust. Inst.* 25 (1994) 883–891.
[41] C.F. Melius, M.E. Colvin, N.M. Marinov, W.J. Pit, S.M. Senkan, *Proc. Combust. Inst.* 26 (1996) 685–692.
[42] E. Pousse, P.A. Glaude, R. Fournet, F. Battin-Leclerc, *Combust. Flame* 156 (2009) 954–974.

Please cite this article in press as: Z. Wang et al., *Proc. Combust. Inst.* (2012), http://dx.doi.org/10.1016/j.proci.2012.05.006